Crystal structure of the ubiquitin binding domains of rabex-5 reveals two modes of interaction with ubiquitin

Penengo, Lorenza ; Mapelli, Marina ; Murachelli, Andrea G ; Confalonieri, Stefano ; Magri, Laura ; Musacchio, Andrea ; Di Fiore, Pier Paolo ; Polo, Simona ; Schneider, Thomas R

DOI: https://doi.org/10.1016/j.cell.2006.02.020

Cell

Crystal Structure of the Ubiquitin Binding Domains of Rabex-5 Reveals Two Modes of Interaction with Ubiquitin

Lorenza Penengo,[1,4] Marina Mapelli,[1,4] Andrea G. Murachelli,[1,4] Stefano Confalonieri,[1] Laura Magri,[1] Andrea Musacchio,[2] Pier Paolo Di Fiore,[1,2,3,*] Simona Polo,[1,2,*] and Thomas R. Schneider[1,2,*]
[1] IFOM, the FIRC Institute for Molecular Oncology Foundation, Via Adamello 16, 20139 Milan, Italy
[2] European Institute of Oncology, Via Ripamonti 435, 20141 Milan, Italy
[3] University of Milan, 20122 Milan, Italy
[4] These authors contributed equally to this work.
*Contact: pierpaolo.difiore@ifom-ieo-campus.it (P.P.D.F.); simona.polo@ifom-ieo-campus.it (S.P.); thomas.schneider@ifom-ieo-campus.it (T.R.S.)
DOI 10.1016/j.cell.2006.02.020

SUMMARY

The interaction between ubiquitinated proteins and intracellular proteins harboring ubiquitin binding domains (UBDs) is critical to a multitude of cellular processes. Here, we report that Rabex-5, a guanine nucleotide exchange factor for Rab5, binds to Ub through two independent UBDs. These UBDs determine a number of properties of Rabex-5, including its coupled monoubiquitination and interaction in vivo with ubiquitinated EGFRs. Structural and biochemical characterization of the UBDs of Rabex-5 revealed that one of them (MIU, *m*otif *i*nteracting with *u*biquitin) binds to Ub with modes superimposable to those of the UIM (*u*biquitin-*i*nteracting *m*otif):Ub interaction, although in the opposite orientation. The other UBD, RUZ (*R*abex-5 *u*biquitin binding *z*inc *f*inger) binds to a surface of Ub centered on $Asp58_{Ub}$ and distinct from the "canonical" $Ile44_{Ub}$-based surface. The two binding surfaces allow Ub to interact simultaneously with different UBDs, thus opening new perspectives in Ub-mediated signaling.

INTRODUCTION

Ubiquitination regulates protein stability and function, with impact on numerous cellular phenotypes. One paramount function of ubiquitin (Ub) is to determine proteolysis of intracellular proteins. In this process, a Ub chain, composed of at least four Ub branching from K48, is appended to target proteins that are then delivered to the proteasome for degradation (Pickart, 2001). Nonproteolytic functions of Ub rely on monomeric Ub or poly-Ub chains branched from lysines other than K48. In this case, ubiquitination affects the structure, the activity, or the localization of the target protein, thereby regulating processes, such as DNA repair (Sun and Chen, 2004), NF-kB-mediated transcription (Chen, 2005), and endocytosis and trafficking (Hicke and Dunn, 2003). The functions of Ub largely depend on its protein-interaction ability. Many proteins (Ub receptors) harbor Ub binding domains/motifs (UBD), which interact with mono- and/or polyubiquitin chains (Hicke et al., 2005). Thus, ubiquitinated proteins and Ub receptors constitute a signaling network within the cell. Some UBDs (CUE, UIM, GAT) can also sustain a process, termed coupled monoubiquitination, whereby a Ub receptor becomes itself monoubiquitinated, through mechanisms that are still largely obscure (see Hicke et al. [2005] for proposed models).

To date, eleven families of UBDs have been identified (Bienko et al., 2005; Hicke et al., 2005). For six of them, the three-dimensional structure of at least one member has been solved, either alone or in complex with Ub. Three UBDs, CUE, UBA, and GAT, although unrelated at sequence level, display similar structural features, as they fold into a three helix bundle with two helices contacting Ub (Kang et al., 2003; Kawasaki et al., 2005; Ohno et al., 2005; Prag et al., 2005). The UIM is a single α helix that packs against Ub (Fisher et al., 2003; Swanson et al., 2003); while the UEV folds into an α/β structure contacting Ub through two loops and part of the β sheet (Pornillos et al., 2002; Sundquist et al., 2004). Finally, the NZF is a zinc finger domain that contacts Ub through residues intercalating the cysteines that coordinate the metal atom (Alam et al., 2004; Wang et al., 2003).

Despite these structural differences and their likely unrelated evolutionary origins, UBDs show remarkable convergence in the mode of interaction with Ub, which is determined by contacts between a hydrophobic surface on the UBD and a hydrophobic pocket centered on Ile44 on Ub. In almost all characterized cases, Ile44 contacts an extremely conserved residue that is specific for each type of UBD (Hicke et al., 2005). Variations on this theme are known. In the case of UBM, a recently described

UBD, the binding to the "classical" hydrophobic patch on Ub is displaced toward Leu8 and apparently does not involve Ile44 (Bienko et al., 2005). These findings explain why the Ile44 "face" of Ub has been totally conserved from yeast to mammals. The extreme conservation of Ub, however, extends to the entire molecule, suggesting that other portions of its surface might be involved in interactions.

The *S. cerevisiae* protein Vps9p is a guanine nucleotide exchange factor (GEF) that regulates the activity of the Rab-like GTPase Vps21 (Hama et al., 1999). Its mammalian ortholog, Rabex-5, regulates the activity of the Rab5 GTPase (Horiuchi et al., 1997). Yeast Vps9p harbors a CUE domain, which interacts with Ub (Kang et al., 2003; Prag et al., 2003) and determines coupled monoubiquitination of Vps9p (Davies et al., 2003; Shih et al., 2003). Moreover, the CUE domain of Vps9 appears to inhibit in *cis* its GEF activity (Donaldson et al., 2003; Shih et al., 2003). Mammalian Rabex-5 displays a region of limited sequence similarity with the CUE of yeast Vps9p (Donaldson et al., 2003); however, it is doubtful whether this region is a bona fide CUE domain and whether Rabex-5 is a true Ub interactor and/or a ubiquitinated protein. Thus, while models for Ub-mediated regulation of Vps9p activity can be put forward (Davies et al., 2003; Di Fiore et al., 2003; Donaldson et al., 2003; Shih et al., 2003), it is unclear whether Rabex-5 is subjected to the same kind of regulation. The present studies were undertaken to shed light on the Ub binding abilities of Rabex-5 and their regulatory role.

RESULTS

Ub Binding Ability of Rabex-5

Rabex-5 displays from N to C terminus (Figure 1A) a zinc finger module, belonging to the ZnF_A20 family (Opipari et al., 1990); a Vps9 domain, which encodes for the Rab5-GEF catalytic activity; and a putative CUE domain. Using a panel of deletion mutants in in vitro pull-down experiments, we found that Rabex-5 binds to Ub through two independent regions, while its putative CUE is not a UBD (Figure 1A and see Figure S1 in the Supplemental Data available with this article online). The first Ub binding region (aa 2–49) corresponds to the ZnF_A20 domain. Thus, a third type of zinc finger domain is able to bind to Ub, besides the NZF and the PAZ domains (Hicke et al. [2005] and references within). Henceforth, we refer to this domain as RUZ domain (*R*abex-5 *u*biquitin binding *z*inc finger). The second region interacting with Ub (aa 48–74) is adjacent to the RUZ and does not contain any evident sequence similarity with known domains.

Characterization of the MIU

The region from aa 48 to 74 of Rabex-5 is well conserved in vertebrates (Figures 1B and S2; Table S1). Secondary structure prediction highlights a putative amphipathic α helix from aa 51 to 70, wherein a signature can be identified (D-ϕ-x-LA-x-x-L-x-x-E-E) that resembles the signature of a UIM (Hofmann and Falquet, 2001; Polo et al., 2003) in a reversed primary sequence orientation (Figure 1B). This suggested that this region of Rabex-5 represents a novel UBD. Within the 48–74 region, Ala58 lays in a position (Figure 1B) similar to that occupied in UIMs by an Ala residue critical for Ub binding (Swanson et al., 2003). Mutagenesis of this residue to Gly, in full-length (FL) Rabex-5, reduced binding to Ub (Figure 1C). In addition, the RUZ-less 48–491 mutant, bearing the additional A58G mutation, showed no detectable Ub binding (Figure 1C). Thus, the 48–74 region of Rabex-5 corresponds to a UBD, which we named MIU (*m*otif *i*nteracting with *U*b).

We searched for other MIU-containing proteins, and found 73 putative MIUs in 62 proteins from all species (Figure S3; Table S2). Prompted by these findings, we tested three putative MIUs from Myosin VI and RNF168 and found that they all bind to polyUb chains linked by K48 or K63 (Figure 1D, left and right panels, respectively). Mutation of the critical Ala to Gly strongly reduced the binding of all tested MIUs (Figure 1D). Interestingly, binding to K48- or K63-linked chains was differently affected by the mutations (Figure 1D). Whether this reflects selective preferences of various MIUs for different Ub chains, as shown for other UBDs (Raasi et al., 2004; Varadan et al., 2004), remains to be established.

The MIU Sustains Coupled Monoubiquitination of Rabex-5

A characteristic of some UBD-containing proteins is to undergo monoubiquitination in a process that depends on the integrity of the UBD itself, named coupled monoubiquitination (Hicke et al., 2005). To check whether the UBDs of Rabex-5 can sustain this process, we coexpressed FLAG-tagged Rabex-5, together with HA-tagged Ub, and found that Rabex-5 is indeed monoubiquitinated in vivo (Figure 1E). Next, we tested mutants displaying either a mutation in the MIU (Rabex-5-A58G), the deletion of the RUZ (48–491), or the double mutation (48–491-A58G). The deletion of RUZ did not significantly affect the ability of Rabex-5 to undergo monoubiquitination. Conversely, the A58G mutation severely reduced monoubiquitination of the FL protein or of the RUZ-deleted mutant (Figure 1E). Thus, the MIU sustains coupled monoubiquitination of Rabex-5.

Rabex-5 Binds to Ubiquitinated EGFR through its UBDs

We searched for physiological partners of the UBDs of Rabex-5. As shown in Figures 2A and 2B, both FLAG-tagged Rabex-5 and endogenous Rabex-5 could coimmunoprecipitate endogenous EGFR, in a ligand-dependent fashion. In addition, GFP-tagged Rabex-5 was recruited to the plasma membrane upon EGF treatment and remained colocalized with EGFR at several stations of the endocytic pathway (Figures 2C and S4).

Rabex-5 preferentially associated with high-molecular weight forms of EGFR, probably representing the

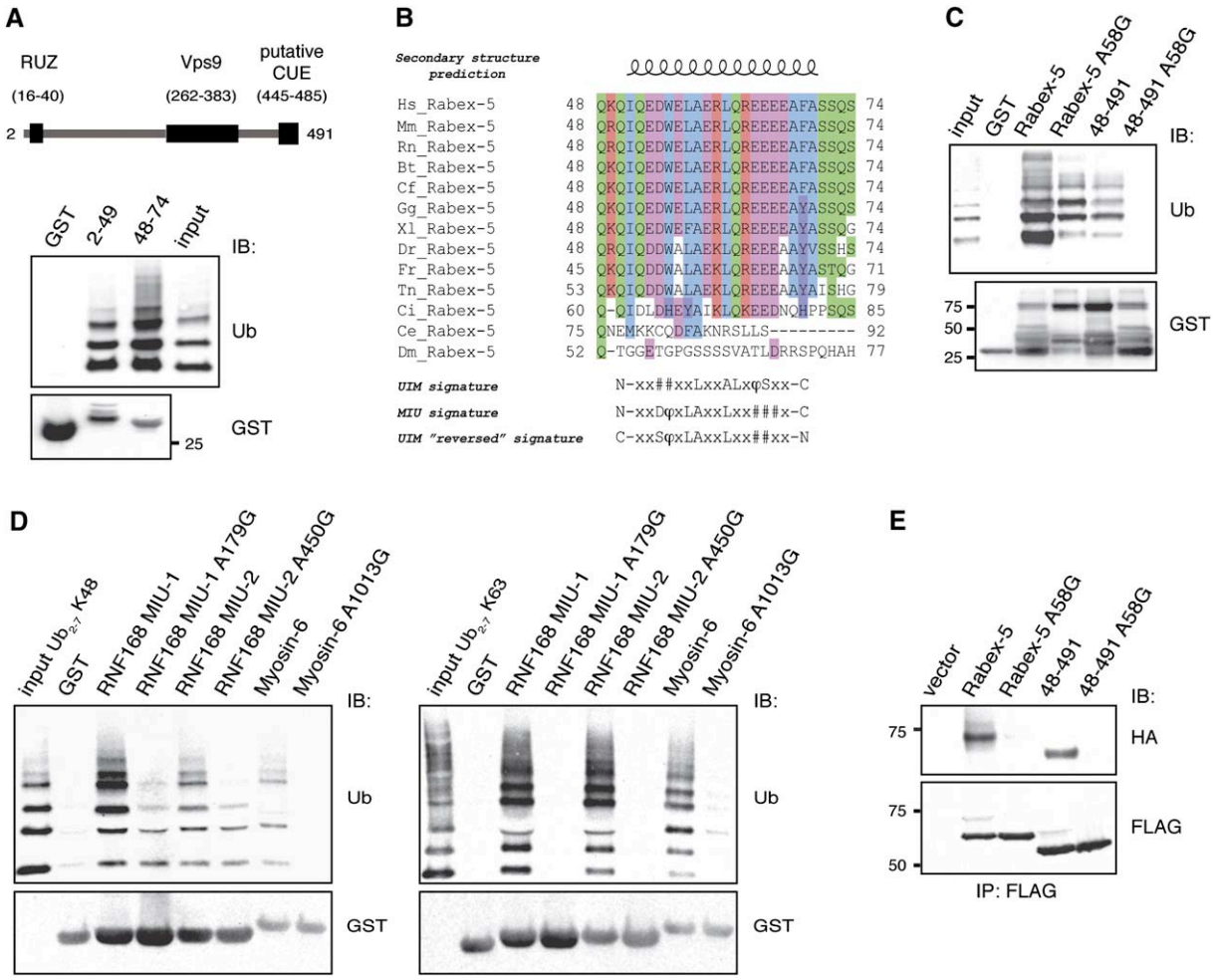

Figure 1. Rabex-5 Binds to Ub

(A) Top, schematic of Rabex-5. Amino acid positions and domains are indicated. Bottom, in vitro pull-down assay using the indicated GST-tagged Rabex-5 constructs (see also Figure S1). GST-fusion proteins were incubated with synthetic polyUb$_{2-7}$ linked by K48 and analyzed in immunoblot (IB) as indicated.

(B) Alignment of human Rabex-5 (aa 48–74) with its orthologs from different organisms (see also Figure S2; Table S1). The secondary structure prediction by SAM-T02 (Karplus et al., 1998) of Rabex-5 fragment 48–74 is depicted above the alignment (α helix, curly line). The signatures of MIU, UIM, and of a reversed UIM are shown; ϕ, large hydrophobic; #, acidic; x, any aa. Abbreviations are as in Figure S3.

(C) In vitro pull-down assay with the indicated Rabex-5 constructs performed as in (A).

(D) In vitro pull-down assay of polyUb$_{2-7}$ linked by K48 (left) or K63 (right) with the indicated GST-MIU fusion proteins (RNF168 MIU-1, aa 168–191; RNF168 MIU-2, aa 439–462; Myosin VI, aa 998–1031; see Supplemental Experimental Procedures for details). IB was as indicated.

(E) HeLa cells were transfected with the indicated FLAG-tagged Rabex-5-based constructs, together with HA-tagged Ub. Twenty-four hours after transfection, cellular lysates (0.5 mg, obtained in a buffer containing 1% Triton X-100, 1% sodium deoxycholate, 0.1% SDS, to reduce coIP of undesired Ub-containing proteins) were immunoprecipitated (IP) and IB as indicated.

ubiquitinated receptor (Figure 2D). To verify this possibility, we overexpressed, in HeLa cells, either Cbl—the E3 ligase that ubiquitinates EGFR—or its dominant-negative version 70Z-Cbl, that markedly reduces ubiquitination of the receptor (Yokouchi et al., 1999). Overexpression of Cbl significantly increased the Rabex-5:EGFR interaction, while the presence of 70Z-Cbl severely reduced it (Figure 2E). Finally, we tested the impact of the Rabex-5 UBDs on the interaction. The double mutant, Rabex-5 48–491 A58G, did not show appreciable interaction with EGFR, whereas the presence of either a functional RUZ (Rabex-5 A58G) or a functional MIU (Rabex-5 48–491) was sufficient for binding to the EGFR (Figure 2F). We concluded that, in vivo, both the RUZ and the MIU are able to engage ubiquitinated EGFR.

Structure of the Tandem RUZ-MIU in Complex with Ub

We determined the crystal structure of the RUZ-MIU fragment of Rabex-5 (aa 2–74, henceforth RUZ-MIU) in

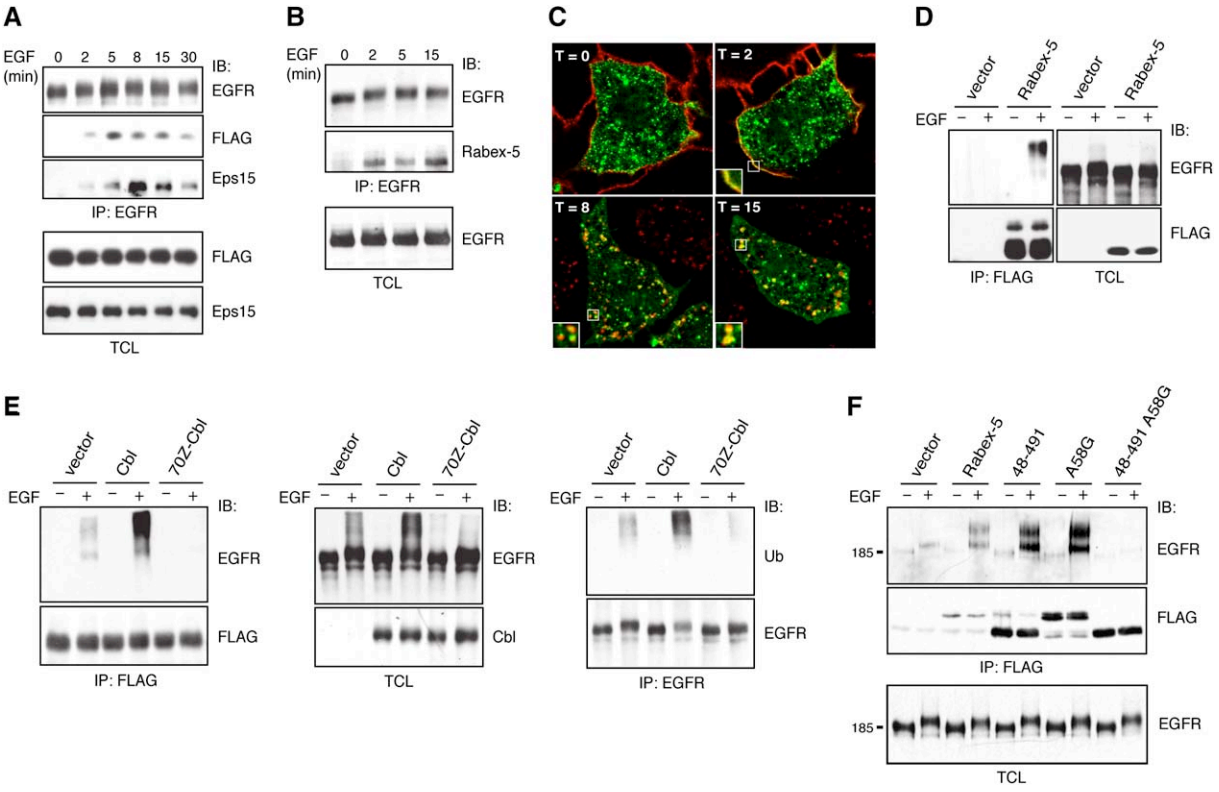

Figure 2. Rabex-5 Binds EGFR through Its UBDs

(A) HeLa cells, transfected with FLAG-Rabex-5, were stimulated with EGF (100 ng/ml) for the indicated time points (min). Lysates (1 mg) were IP and IB as indicated. TCL, total cellular lysate.

(B) HeLa cells, not transfected, were processed as in (A).

(C) HeLa cells, transfected with GFP-Rabex-5, were incubated (1 hr, on ice) with the 13A9 anti-EGFR antibody. After wash and addition of EGF (100 ng/ml), cells were shifted to 37°C for the indicated time points (T, min). 13A9 was detected with Cy3-conjugated secondary antibody (red). Central sections obtained by confocal microscopy are shown. Merged channels are shown (see also Figure S4). The boxed areas are magnified in the insets.

(D) HeLa cells, transfected as indicated, where stimulated with EGF (100 ng/ml, 5 min). Lysates (1 mg) were IP and IB as indicated.

(E) HeLa cells, stably transfected with Cbl, 70Z-Cbl, or empty vector, were treated with EGF (as in [D]). IP and IB were as indicated.

(F) HeLa cells, transfected with the indicated FLAG-tagged Rabex-5 constructs, were treated with EGF (as in [D]). IP and IB were as indicated. Note that, in this experiment, coIP of FL-Rabex-5 with EGFR appears reduced, as compared to that of the Rabex-5 A58G and Rabex-5 48–491 mutants, because less Rabex-5 was IP (see IB: FLAG panel). However, when corrected for the amount of protein IP, all three proteins display comparable interaction with EGFR.

complex with Ub in two crystal forms. Form I is hexagonal and contains one molecule of RUZ-MIU and one molecule of Ub per asymmetric unit, while form II is triclinic with six copies of each molecule in the unit cell. Both structures were solved exploiting the anomalous signal from the Zn^{2+} ion and refined to 2.4 and 2.1 Å resolution (Table S3), respectively. Representative electron density maps are shown in Figures 4D and 5B. In both structures, all molecules of RUZ-MIU assume similar conformations. The ordered part of the elongated molecule begins at residue $Leu17_{Rbx}$ and folds, as predicted for the A20-type zinc fingers (Wertz et al., 2004), into a treble clef motif (Krishna et al., 2003). This is followed by a helix that harbors the second Ub binding site (Figure 3A).

Within each RUZ-MIU molecule, the RUZ and MIU domains contact two different molecules of Ub (Figure 3A); conversely, every molecule of Ub contacts two molecules of RUZ-MIU again using two disjoint surfaces (Figure 3A).

Comparison of the conformation of the seven crystallographically independent copies of RUZ-MIU identified two regions, corresponding to the RUZ (residues $Leu18_{Rbx}$ to $Trp39_{Rbx}$) and the MIU plus some flanking residues (residues $Arg40_{Rbx}$ to $Glu64_{Rbx}$), which are separated by a flexible hinge (Figure 3B). Superposition of the different copies of the individual regions yields rmsds (root-mean-square deviations) between 0.2 and 0.3 Å for Cα atoms, indicating that the conformations are, given the coordinate uncertainties of the structures (Table S3), identical within error. RUZ-MIU can thus be considered as consisting of two rigid domains that are joined together between residues $Trp39_{Rbx}$ and $Arg40_{Rbx}$. The relative orientation of the two domains is dictated by crystal packing forces,

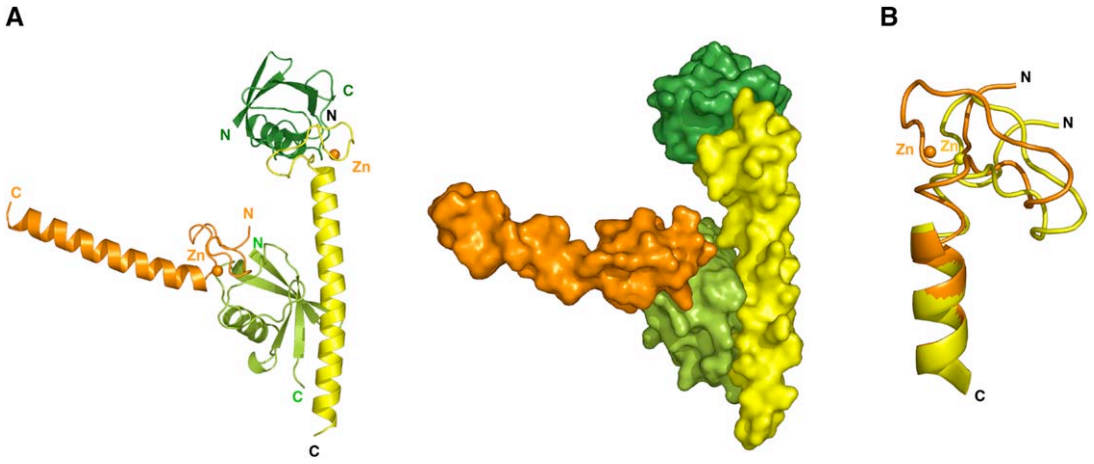

Figure 3. Overview of the Structure

(A) Secondary structure diagram (left) and surface representation (right) of two molecules of RUZ-MIU (yellow and orange) in complex with two molecules of Ub (light green and dark green). The Zn^{2+} ions of Rabex-$5_{2–74}$ are drawn as orange spheres.

(B) Superposition of two molecules of RUZ-MIU, orange and yellow. Residues 40–64_{Rbx} are shown as a helix, while for residues 17–39_{Rbx} the backbone trace is indicated by a tube; Zn^{2+} ions are drawn as spheres.

whereby steric considerations preclude the simultaneous binding of a RUZ and a MIU domain of the same Rabex-5 molecule to one Ub molecule (Figure S5).

The RUZ Domain Folds as a Treble Clef and Binds to a Region of Ub Different from the Ile44 Patch

Residues $Leu17_{Rbx}$ to $Trp39_{Rbx}$ represent a Cys2/Cys2 zinc finger domain of the A20-type. The first pair of cysteines ($Cys19_{Rbx}$ and $Cys23_{Rbx}$) forms a zinc knuckle and the second pair of cysteines ($Cys35_{Rbx}$ and $Cys39_{Rbx}$) is located on the N-terminal turn of the helix (Figure 4A). This arrangement of Zn ligands is characteristic of the treble clef zinc finger motif. However, other features of the treble clef motif, notably β hairpin structures before the first cysteine and in the loop between the second and the third cysteine, are absent in the structure of RUZ-MIU. Despite the lack of regular secondary structure elements, the region between $Cys23_{Rbx}$ and $Cys39_{Rbx}$ is structurally well defined due to the presence of an intricate network of hydrogen bonds and salt bridges (Figure 4A).

The RUZ is conserved in Rabex-5 from different vertebrates (Figure 4B). Characteristic elements such as a particular arrangement of glycines and prolines, needed for the compact fold of the RUZ, are conserved in zinc fingers present in nonvertebrates such as parasites and plants (Figure 4B). Some A20-type zinc fingers exhibit close similarity with the RUZ motif, while others, such as Hs_A20.6 (Figure 4B) share only a similar spacing between the cysteine residues.

The RUZ contacts Ub in a region centered on $Asp58_{Ub}$ (Figure 4C). As shown in the representative electron density map (Figure 4D), the central residue in the binding interface is $Ser36_{Rbx}$, which forms hydrogen bonds to both carboxylate oxygens of $Asp58_{Ub}$ with its amide nitrogen (2.9 Å) and its Oγ-atom (2.6 Å). $Asp58_{Ub}$ itself connects back to $Tyr26_{Rbx}$-N via its carbonyl oxygen (3.0 Å). Further polar interactions are formed between $Cys35_{Rbx}$-Sγ and $Arg54_{Ub}$-NH2 (3.3 Å), between $Tyr25_{Rbx}$-OH and $Glu51_{Ub}$-Oε2 (2.8 Å), and between $Asn28_{Rbx}$-N and $Ser57_{Ub}$-Oγ (3.3 Å). The binding between the two molecules is further strengthened by stacking interactions between the side chains of $Tyr25_{Rbx}$ and $Arg54_{Ub}$ (Figure 4E).

The MIU Binds to Ub through UIM-like Interactions with Reversed Chain Orientation

The second Ub binding site on RUZ-MIU is located on the helical part of the structure and encompasses residues from seven turns of the helix starting with $Arg47_{Rbx}$ and ending with $Phe69_{Rbx}$. Overall, the binding mode resembles that of the complex between Vps27-UIM and Ub (Swanson et al., 2003), with the striking difference that the helix binding to Ub is accommodated in the opposite direction, i.e., the C terminus of Ub is pointing in the direction of the C terminus of the UBD while in the Vps27-UIM:Ub complex the C terminus of Ub points toward the N terminus of the UBD Ub (Swanson et al., 2003; Figure 5A). As in the Vps27-UIM:Ub complex, at the center of the binding interface, $Ala58_{Rbx}$ (Ala266 Vps27-UIM) is inserting its methyl group into a hydrophobic depression built by $Leu8_{Ub}$, $Ile44_{Ub}$, $His68_{Ub}$, and $Val70_{Ub}$ (Figure 5B).

In UIMs another invariant amino acid is represented by a serine residue at position +4, with respect to the central alanine, which has been described to play an important role for the binding of the UIM of Vps27 and Hrs to Ub (Fisher et al., 2003; Shih et al., 2002; Swanson et al., 2003). In the NMR structure of the Vps27-UIM:Ub complex, it was found that the hydroxyl oxygen of $Ser270_{Vps27}$ is forming hydrogen bonds with the amide nitrogens of $Ala46_{Ub}$ and/or $Gly47_{Ub}$ (Swanson et al., 2003). In Rabex-5, the position equivalent to $Ser270_{Vps27}$ is occupied

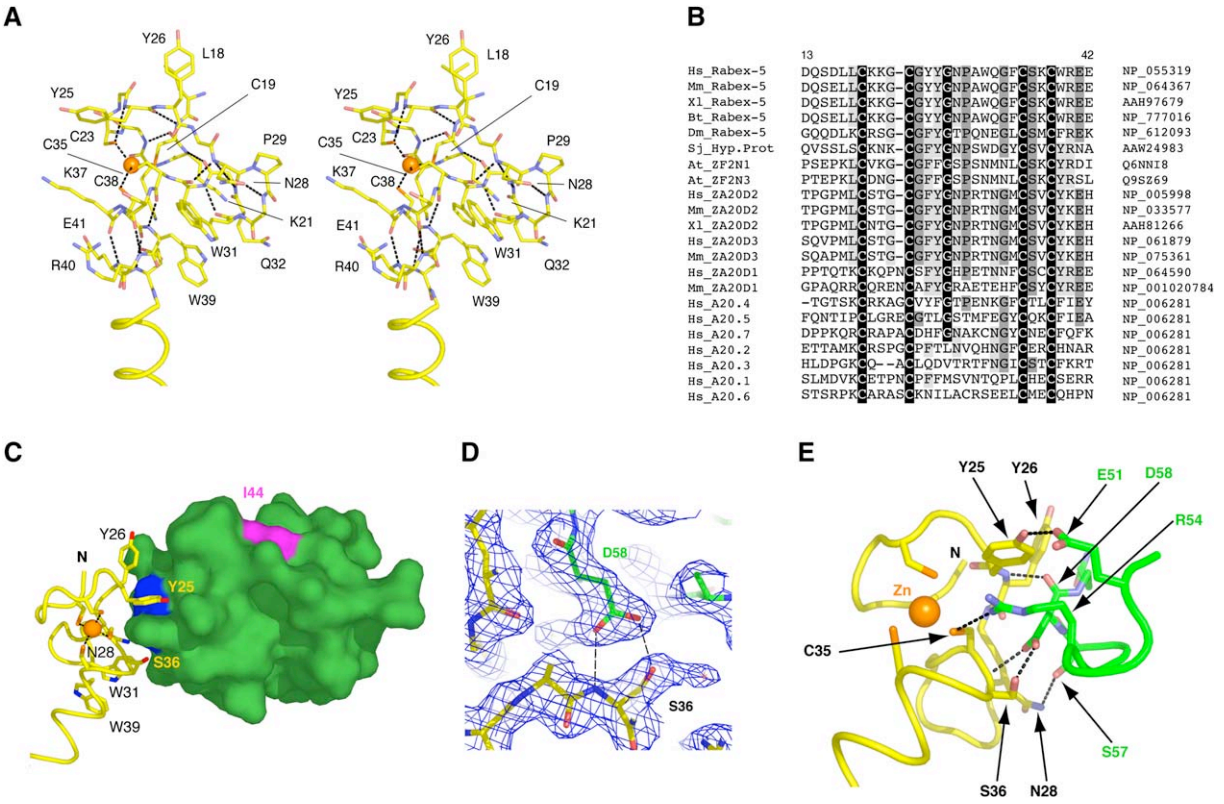

Figure 4. The RUZ Binds to an Ub Surface Centered on Asp58

(A) Stereoview of the treble clef zinc finger domain of Rabex-5. Residues from 18 to 41 are shown in ball-and-sticks; hydrogen bonds are depicted as black dashed lines.

(B) Alignment of representative ZnF_A20 domains. GenBank accession numbers are shown on the right. Numbers on top refer to human Rabex-5. The multiple ZnF_A20 domains in the A20 protein are indicated by their numbers. Abbreviations are as in Figure S3.

(C) Schematic representation of the binding between RUZ (yellow) and Ub (green surface). The locations of $Ile44_{Ub}$ and $Asp58_{Ub}$ are indicated on the surface of Ub in magenta and blue, respectively.

(D) $2F_{obs} - 1F_{calc}$ difference electron density contoured at the 1σ level around residue $Asp58_{Ub}$ (green) and residue $Ser36_{Rbx}$ (yellow). Hydrogen bonds are indicated by dashed black lines.

(E) Hydrogen bonds and salt-bridge interactions between Rabex-5 (yellow) and Ub (green).

by $Asp54_{Rbx}$ whose carboxylate group is positioned such that both oxygens can simultaneously engage in separate hydrogen bonds with the amide nitrogens of $Ala46_{Ub}$ and $Gly47_{Ub}$ (Figures 5C and 5D) leading to a tighter binding. Shih et al. (2002) showed that mutation of Ser270 into Asp in Vps27 reduced 5- to 6-fold the Ub binding ability of the Vps27-UIM. An explanation for this apparent contradiction came by the superimposition of the structures (Figure 5D). The amide group of $Gln50_{Rbx}$, which in the Rabex5-MIU:Ub complex fixates the $Asp54_{Rbx}$-carboxylate in an optimal position via a salt bridge, is not present in Vps27-UIM:Ub complex, where $Ser274_{Vps27}$ substitutes for $Gln50_{Rbx}$.

The third region of importance in both UIM and MIU binding is a group of glutamates C-terminal (MIU) or N-terminal (UIM) of the central Ala. In both motifs, one of the glutamates forms polar interactions with $Arg42_{Ub}$ and/or $Arg72_{Ub}$. In the MIU-Ub complex, the carboxylate group of $Glu65_{Rbx}$ forms not only a salt bridge to $Arg42_{Ub}$ but also accepts a hydrogen bond from the amide nitrogen of $Leu73_{Ub}$. The latter interaction, together with a hydrophobic interaction between $Phe69_{Rbx}$ and the side chain of $Leu73_{Ub}$ tacks the C terminus of Ub up to $Leu73_{Ub}$ to Rabex-5 (Figure 5C).

N-terminal of $Asp54_{Rbx}$, two more residues of Rabex-5 are involved in specific contacts to Ub and extend the binding surface. The amide moiety of $Gln50_{Rbx}$ donates a hydrogen bond to the carbonyl oxygen of $Thr66_{Ub}$, and the guanidinium group of $Arg47_{Rbx}$ forms a hydrogen bond with the carbonyl oxygen of $Lys63_{Ub}$ (Figure 5C). Thus, in total, the resulting binding region for the MIU involves seven turns of the α helix.

Validation of the Two Surfaces of Interaction between Rabex-5 and Ub

The structure of the RUZ-MIU:Ub complex reveals that the two UBDs are able to interact with distinct surfaces on Ub, centered on $Asp58_{Ub}$ and $Ile44_{Ub}$, respectively. We tested

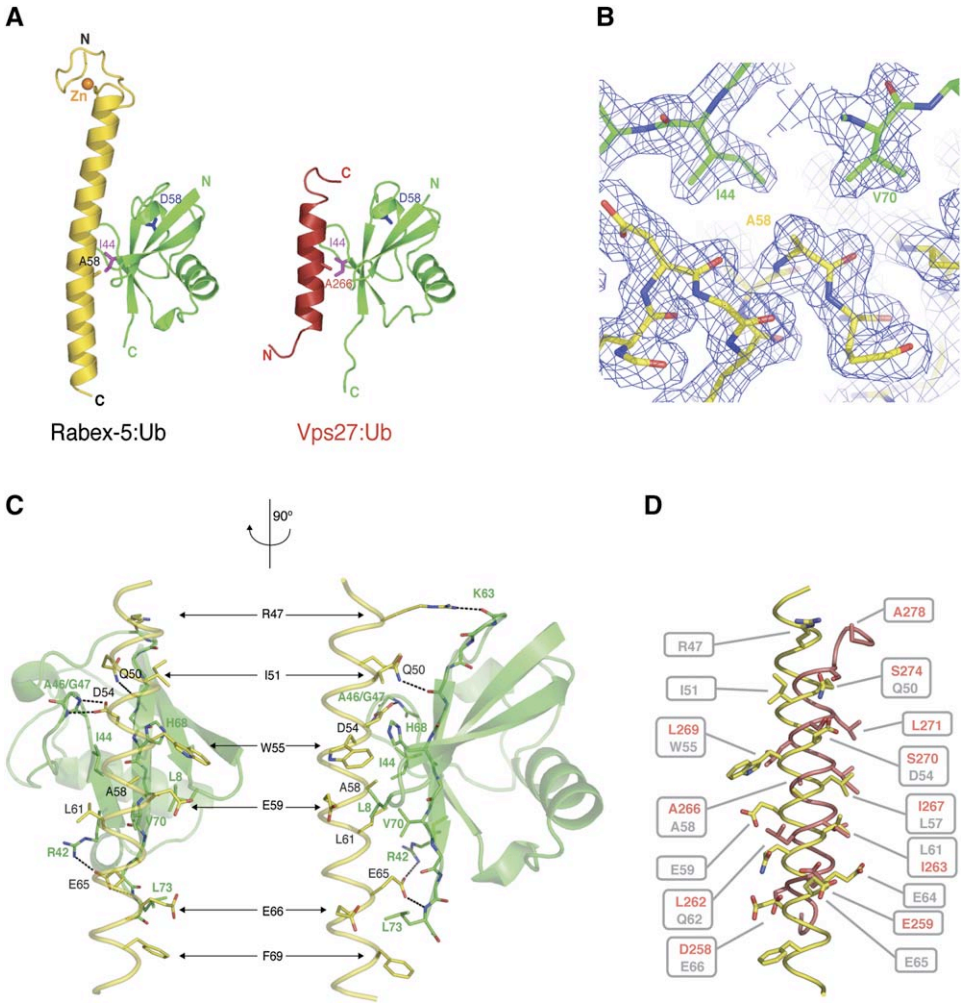

Figure 5. The MIU:Ub Complex Resembles the UIM:Ub Complex

(A) Structures of the Rabex-5-MIU:Ub (yellow and green) and the Vps27-UIM:Ub (red and green) complexes.

(B) $2F_{obs} - 1F_{calc}$ difference electron density contoured at the 1σ level around residue $Ala58_{Rbx}$ (yellow) and residues $Ile44_{Ub}$ and $Val70_{Ub}$ (green).

(C) Interactions between Ub (green) and MIU (yellow). Hydrogen bonds and salt bridges are indicated by dashed black lines.

(D) Ub binding residues of the MIU of Rabex-5 (yellow) and of the UIM of Vps27 (red). Models of the RZF-MIU:Ub complex and the Vps27-UIM:Ub complex (Swanson et al., 2003) were superimposed based on residues 5–70 of the Ub molecules. Side chains involved in interaction between MIU (yellow)/UIM (red) and Ub are shown in stick representation.

two Ub mutants, Ub-I44A and Ub-D58A, for binding to Rabex-5. The I44A mutation strongly reduced the binding of Ub to the MIU but not to the RUZ, while the D58A mutation had the complementary effect (Figure 6A). Next, we analyzed mutants in either the RUZ or the MIU. In the context of the isolated RUZ (aa 2–49), we mutagenized Tyr25 to Phe to prevent the formation of the hydrogen bond between the $Tyr25_{Rbx}$-OH and $Glu51_{Ub}$. We also employed the already-described mutant, A58G, in the context of the isolated MIU (aa 48–74). Both mutants displayed strongly reduced binding to monomeric Ub (Figure 6B).

Next, we characterized the interaction of the Rabex-5 UBDs with monomeric Ub, by isothermal titration calorimetry (ITC). The dissociation constants were 12.0 μM for the RUZ:Ub interaction and 28.7 μM for the MIU:Ub one (Figures 6C and S6). The reactions were exothermic, with a stoichiometry of 1:1.

The RUZ-MIU fragment displayed an apparent K_D for interaction with Ub of 6 μM, comparable to those of the isolated domains. This confirms that the two UBDs of Rabex-5 are oriented in a way that precludes their simultaneous binding to a single molecule of Ub, a condition under which a K_D in the low nanomolar range would be predicted. Finally, the introduction of the A58G mutation in the RUZ-MIU resulted in a 3-fold reduction in the affinity; conversely, the Y25F mutation did not significantly affected the K_D of the RUZ-MIU:Ub interaction, likely because of residual stacking interactions (Figures 6C and S6).

Of note, the ITC data suggest a 1:1 stoichiometry for the RUZ-MIU:Ub complex (Figure 6C), a finding not

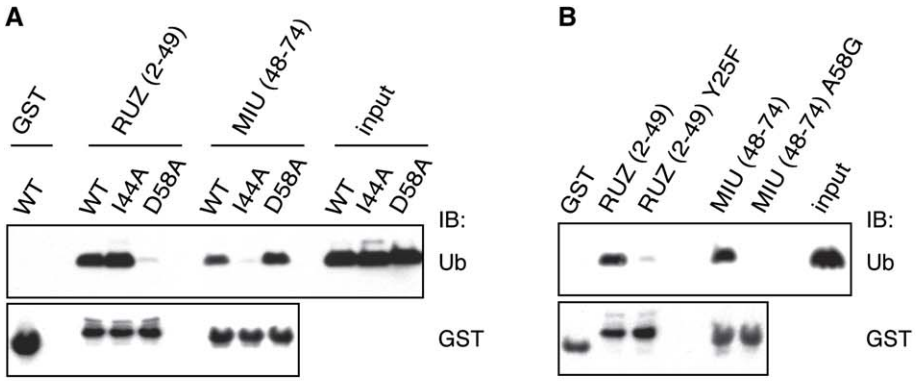

C

Interaction	K_B ($10^4 M^{-1}$)	K_D ($10^{-6} M$)	ΔH^{obs} (10^3kcal/mol)	$T\Delta S$ (10^3kcal/mol)	ΔG^{obs} (10^3kcal/mol)	N
MIU (48-74) + Ub	3.5	28.7	- 16.9	- 10.8	- 6.2	1.0
RUZ (1-49) + Ub	8.3	12.0	- 15.7	- 9.2	- 6.5	0.9
RUZ-MIU (1-74) + Ub	15.7	6.4	- 25.6	- 18.6	- 7.0	1.0
RUZ-MIU^{A58G} (1-74) + Ub	5.3	18.8	- 22.1	- 15.7	- 6.4	1.1
RUZ^{Y25F}-MIU (1-74) + Ub	15.9	6.3	- 28.9	- 21.8	- 7.1	1.2

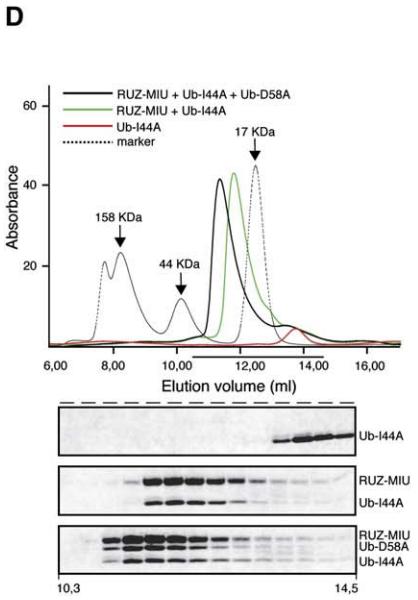

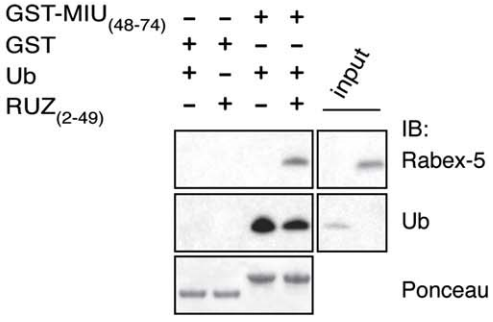

Figure 6. Validation of the Two Surfaces of Interaction between Rabex-5 and Ub

(A) Ub wt, Ub-I44A, and Ub-D58A were used in an in vitro pull-down assay with the indicated GST constructs of Rabex-5. Samples were resolved by Tricine-PAGE and IB as indicated.

(B) GST-RUZ (aa 2–49), GST-MIU (aa 48–74), and their indicated mutants were used in an in vitro pull-down assay with wt Ub. Detection was as in (A).

(C) Determination of binding affinities for Rabex-5 with Ub by ITC. Thermodynamic parameters for the interaction of the UBDs of Rabex-5 with Ub were derived from experiments performed as described in Supplemental Experimental Procedures. K_B, binding constant; K_D, dissociation constant; ΔH^{obs}, observed binding enthalpy; ΔS, binding entropy; ΔG^{obs}, observed Gibbs' free energy; N, binding stoichiometry.

(D) Stoichiometry of the RUZ-MIU:Ub complex. One hundred μM purified RUZ-MIU was incubated (1 hr, 20°C) with either Ub-I44A (100 μM) or Ub-I44A/Ub-D58A (100 μM each), followed by fractionation on a Superdex75 column (Amersham). Fractions from 10.3 to 14.5 ml were separated by Tricine-PAGE and stained with Coomassie (the Ub-D58A variant is retarded because of a 15 residues N-terminal tail).

immediately reconcilable with the structural data. To clarify this point, we analyzed, by size exclusion chromatography, whether Ub-I44A and Ub-D58A, which are respectively impaired in their binding to MIU or RUZ, can simultaneously bind to RUZ-MIU. We observed a peak shift in the elution profile of the RUZ-MIU incubated with equimolar amounts of Ub-I44A and Ub-D58A, as compared to that of the RUZ-MIU:Ub-I44A complex (Figure 6D). This indicates that Ub can enter a 2:1 complex with RUZ-MIU in solution. The apparent 1:1 stoichiometry, detected by ITC, is most likely a networking effect, due to the presence of two binding sites on Ub for RUZ-MIU (see Figure S7 for details and explanations).

The finding that there are two binding surfaces on Ub might have interesting biological implications, if a single Ub moiety were able to contact two different Ub receptors. To investigate this possibility, we performed a binding assay in which GST-MIU (aa 48–74), immobilized onto glutathione-Sepharose beads (GSH), was first incubated with Ub for 1 hr at room temperature and then with purified RUZ (aa 2–49). As shown in Figure 6E, the RUZ domain was efficiently retained on the beads, entering a trimeric complex with the MIU:Ub complex. Thus, Ub can simultaneously interact with two different partners, raising the possibility that in vivo it can bridge together different Ub receptors.

DISCUSSION

In this study, we report the characterization of two UBDs, contained in Rabex-5. These findings not only add to our understanding of the Ub:UBDs interaction but also harbor a number of interesting biological and functional implications. While this manuscript was undergoing review, two papers reported the Ub binding properties (Mattera et al., 2006) and the determination of the structure (Lee et al., 2006) of the N terminus of Rabex-5. The conformation of the molecules, and the interaction surfaces between the N terminus of Rabex-5 and Ub, in this paper and in that from Lee et al. [2006] are in agreement.

The MIU:Ub Interaction

The MIU can be roughly equaled to an inverted UIM. At the level of primary sequence, the MIU did not show significant similarity to the UIM, while it could be aligned rather precisely to a UIM consensus in a reversed orientation (Figure 1B). In addition, the HMM profile of the MIU did not recognize any UIM in the database (Figure S3) and vice-versa (S.C., unpublished data). Accordingly, the MIU binds to Ub in a manner similar to the UIM but with the helix running in the opposite direction (this paper; Lee et al., 2006). In the UIM, the insertion of a methyl group provided by the highly conserved alanine into the hydrophobic depression created on the Ub-surface by Leu8, Ile44, His68, and Val70 identifies an essential contact (Swanson et al., 2003). The MIU uses the same residue, $Ala58_{Rbx}$, to implement this central interaction, and indeed, the mutation of this residue to Gly strongly reduced the binding to Ub.

The MIU:Ub interaction displays higher affinity (K_D ~29 μM) with respect to that between UIMs and Ub (K_Ds ~100–500 μM; Hicke et al., 2005). This is mirrored by structural results that revealed the enforcement of individual contacts and the increase in the number of interactions between MIU and Ub. For example, $Asp54_{Rbx}$ functionally corresponds to Ser270 of the Vps27-UIM. In contrast to the single hydroxyl oxygen of serine, the carboxylate group of $Asp54_{Rbx}$ has the capacity to engage simultaneously in two hydrogen bonds instead of one, thus gaining binding energy. N-terminal of $Ala58_{Rbx}$, the MIU binding interface extends further with interactions mediated by $Gln50_{Rbx}$ and $Arg47_{Rbx}$ resulting in a binding region that involves seven turns of α helix and is significantly larger than the binding region of Vps27-UIM, which involves four turns of α helix. To provide all the interaction partners, the helix of the MIU shows a significant bend in the complex (Figure 5A), which is not seen in the UIM helices (Swanson et al., 2003). Given the size of the MIU-Ub binding interface and its asymmetry, it is unlikely that few sequence alterations could result in a reversal in the orientation of binding, as observed for the SUMO binding motifs of PIASX (Song et al., 2005) and RanBP2 (Reverter and Lima, 2005).

Another common feature of UIM and MIU is their ability to drive coupled monoubiquitination (Hicke et al., 2005; Figure 1E). Although the molecular mechanisms of this phenomenon are still obscure, the ability of the UIM to bind to Ub seems to be a necessary condition (Hicke et al., 2005). It should be mentioned that in the study by Mattera et al. (2006), a role for the Zinc finger domain of Rabex-5 in coupled monoubiquitination was described. Under our conditions of analysis, we did not evidence a major contribution of this domain (Figure 1E).

It is also interesting that in UIM-dependent coupled monoubiquitination, the ubiquitination event seems to occur at Lys residues N-terminal of the UIM (Miller et al., 2004). This has been put in relationship with the antiparallel binding of Ub to the UIM. In the case of the MIU:Ub interaction, the two chains are in the same orientation, raising the possibility that MIU-mediated coupled monoubiquitination occurs C-terminal of the UBD. Indeed, we have evidence that this is the case for Rabex-5 (L.P. and S.P., unpublished data).

Finally, we identified a family of MIU-containing proteins and provided evidence that some of them, including Myosin 6, can bind to Ub. Future work will address whether all MIU-containing proteins are endowed with similar

(E) Five micromolar GST-MIU or GST, immobilized onto GSH beads, was incubated with 20 μM of Ub and then 5 μM of purified RUZ (aa 2–49, cleaved from the GST moiety) was added to the complex. Detection was performed as in (A). Comparable loading of GST-MIU is shown by Ponceau staining (bottom panel). The presence of RUZ on beads was detected by IB with the anti-Rabex-5 antibody G32, which recognizes the first 49 aa of Rabex-5 (see Supplemental Experimental Procedures).

properties and whether they are also subjected to coupled monoubiquitination. In the case of Myosin 6, a series of evidence (reviewed in Frank et al. [2004]) supports a role in membrane trafficking, an area in which the involvement of the Ub network is paramount. Thus, it will be of interest to determine how the Ub binding properties of Myosin 6 regulate its function.

The RUZ:Ub Interaction

The second Ub binding motif in the N-terminal region of Rabex-5 is a Cys2/Cys2 zinc finger of the A20 type. Another Ub binding Zinc finger, the NZF, has been structurally characterized (Alam et al., 2004; Wang et al., 2003). However, RUZ and NZF display different folds and modes of interaction with Ub (Figure S8). RUZ binds Ub on a novel surface centered on $Asp58_{Ub}$ (this paper; Lee et al., 2006). This surface does not overlap either with the "canonical" I44-centered binding surface or with the "shifted" surface (Bienko et al., 2005) responsible for interaction with UBM (Figure S9).

An obvious question is whether all A20-type zinc fingers display Ub binding properties. An alignment of some of these domains (Figure 4B) revealed that the fourth zinc finger domain of the A20 protein, Znf4, displays the closest homology to the RUZ of Rabex-5. In particular, the first aromatic residue after the first pair of cysteines is a tyrosine, both in RUZ and in Znf4 and not a phenylalanine as in many other A20-type zinc fingers. Of note, we show that a Y to F mutation of that position impairs Ub binding. Moreover, the equivalent of $Ser36_{Rbx}$ in the Znf4 is a threonine, which is capable of forming the same interactions as in the RUZ:Ub complex. Thus, the Znf4 of A20 might be endowed with Ub binding properties.

We note that the A20 protein displays both deubiquitinating and Ub ligase (E3) abilities (Wertz et al., 2004). The Znf4 was identified as the critical determinant for the E3 ligase activity (Wertz et al., 2004). In addition, Mattera et al. (2006) and Lee et al. (2006) provided evidence compatible with the possibility that the RUZ domain of Rabex-5 might be endowed with a similar activity. E3 ligases can either possess intrinsic catalytic activity (HECT-type E3s), or function as adaptors between E2 enzymes and substrates (RING-type E3s; Pickart, 2001). In this latter case, actual catalysis is executed by the E2. RUZ domains are unlikely to possess intrinsic catalytic activity and therefore are candidates to be E3 ligases of a RING-like type. Our present results show that the RUZ domain binds to Ub. To reconcile all these observations, one might postulate that RUZ-containing proteins are recruited to ubiquitinated E2 enzymes, thus allowing bridging with hypothetical substrates bound to other regions of the same RUZ-containing proteins. In support of this, Lee et al. (2006) have provided evidence for a Ub-mediated interaction between the RUZ and UbcH5C. Such a scenario could be speculatively extended to various other Ub receptors.

Biological Implications

The Ile44-based surface on Ub surface is involved in literally hundreds of interactions with Ub receptors. Further work will be needed to establish whether the surface centered on Asp58 (this paper; Lee et al., 2006) is similarly promiscuous or involved in more "specialized" functions. Whatever the case, the fact that a single Ub moiety can simultaneously engage two different partners (Figure 6E) adds a new dimension to the complexity of the Ub-based network and provides interesting outlooks. For example, ubiquitination is critical for intracellular trafficking of membrane bound proteins (Hicke and Dunn, 2003). It was suggested that Ub receptors act serially on monoubiquitinated cargoes, during their transport from the cell surface to the lysosome (Hicke et al., 2005). However, all UBDs described so far engage the $Ile44_{Ub}$-based pocket, making such a "hand-off" mechanism difficult to conceptualize. One possibility is that Ub receptors are organized in a hierarchical cascade with increased affinity for Ub. However, our results also open the possibility that Ub receptors with specificity for noncanonical surfaces of Ub are intercalated, in the cascade, to "canonical" Ub receptors, thus facilitating the hand-off of the ubiquitinated cargo. Whether Rabex-5 has such a function remains to be established. In addition, the dual binding ability of Ub might allow recruitment of regulating enzymes, at specific points of the cascade, without compromising the sequential delivery of the ubiquitinated cargo: a possible mechanism well fitting the known regulatory properties of Rabex-5.

In this context, the physical association between Rabex-5 and the EGFR, reported here, identifies an important target of the networking ability conferred upon Rabex-5 by its UBDs. By drawing an analogy with the well-characterized EGFR-Sos1-Ras system, we would like to propose that the interaction with ubiquitinated EGFRs allows relocalization of Rabex-5 to the plasma membrane or to early endosomes (Figure 2C), thereby allowing activation of Rab5. Another Vps9 domain-containing protein, RIN1, has been proposed for this role (Tall et al., 2001), which can be directly recruited to the EGFR through SH2:phosphotyrosine interactions (Barbieri et al., 2003). Rabex-5 and RIN1 could work redundantly; however, it is interesting that they bind to differently post-translationally modified EGFRs, ubiquitinated and phosphorylated, respectively. Recent evidence has suggested that the EGFR might follow different internalization routes, as a function of its ubiquitination status (Sigismund et al., 2005). Thus it is tempting to speculate that differential mechanisms of Rab5 activation by EGFR have evolved in the control (and possibly in the coordination) of different endocytic pathways.

We finally note that, during evolution, Rabex-5 loses a UBD (the CUE) but acquires two novel Ub-interacting surfaces. This is reminiscent of what happens to the UIM-containing protein eps15, which in mammals displays a UIM, while in yeast (Ede1p) displays a UBA domain. This suggests positive pressure on functions rather than on structures and, at the same time, probably the "need" to evolve more complex modes of operation for the Ub-based network. This might, in turn, reflect the challenge of adapting an originally simple signaling system

to the increasing complexity of the endocytic membrane system throughout evolution.

EXPERIMENTAL PROCEDURES

Reagents and Constructs

Antibodies were: anti-Ub (P4D1, Santa Cruz Biotechnology), anti-FLAG and anti-FLAG affinity gel (M2, Sigma), anti-HA (Babco), anti-Rabex-5 monoclonal (G32; see Supplemental Experimental Procedures). Polyubiquitin Lys48- and Lys63-linked chains (2–7 Ub moieties) and bovine ubiquitin, employed in the crystallization studies, were from Boston Biochem. All constructs were engineered by either site-directed mutagenesis or recombinant PCR (see Supplemental Experimental Procedures), and sequence verified.

Biochemical Studies

Transfections were performed using Lipofectamin (Invitrogen). Immunoprecipitation and immunoblotting (Fazioli et al., 1992) and immunofluorescence and internalization assays were performed as described (Sigismund et al., 2005).

GST fusion proteins were expressed and purified as described (Sessa et al., 2005). Cleavage from GST was, as appropriate, with PreScission Protease (Amersham Bioscience, 10 unit/mg of substrate, 16 hr, 4°C), or with biotinylated thrombin (Thrombin Cleavage Capture Kit, Novagen, 1 unit/mg of substrate, 16 hr, RT).

For crystallization studies, the cleaved RUZ-MIU fragment (aa 2–74) was concentrated and loaded on a Superdex75 column (Amersham Biosciences). Fractions containing RUZ-MIU were pooled and incubated for 2 hr at RT with bovine Ub (1:1 molar ratio), followed by concentration and chromatography on a Superdex75 column. Peak fractions were concentrated with Vivaspin concentrators to 20 mg/ml. Usually, 1–2 mg of pure complex was obtained per liter of bacterial culture.

Details of the procedures used for pull-down experiments and ITC assays are in Supplemental Experimental Procedures.

Crystallization and Structure Determination

Crystallization experiments were performed with the sitting drop vapor diffusion technique at 20°C. To screen for initial crystallization conditions, 100 nl of protein solution, at a concentration of 20 mg/ml, was mixed with 100 nl reservoir solution using a Cartesian Honeybee liquid handler (Genomic Solutions) and equilibrated against 150 μl reservoir solution. Rod-shaped hexagonal crystals (form I) grew with a reservoir consisting of 0.2 M Li_2SO_4, 0.1 M MES (pH 6.5), and 25% PEG 3350, while plate-like crystals (form II) grew with a reservoir buffer containing 0.2 M ammonium acetate, 0.1 M NaCitrate (pH 6.5), and 25% PEG 4000. For data collection, crystals were gradually transferred to a cryo-buffer (reservoir buffer supplemented with 20% glycerol) and flash-cooled in liquid N_2. All data used in structure solution and refinements were collected on beamlines ID29 and BM14 at ESRF (Grenoble, France). Data collection statistics are shown in Table S1. For both crystal forms, all data were collected from one crystal. Data were integrated and scaled with HKL2000 (Otwinowski and Minor, 1997) and merged with XPREP (Bruker AXS).

Initial phases were derived using the combination of SHELXC, SHELXD, and SHELXE (Sheldrick, 2002) with default parameters from the HKL2MAP graphical user interface. For crystal form I, model building was initiated with a helical fragment placed into the electron density by the HelixBuild module of ArpWarp (Morris et al., 2002). For crystal form II, a first model containing 438 residues was automatically built into the electron density by ArpWarp. Subsequent cycles of model building and refinement were performed with Xfit (McRee, 1999) and CNS (Brunger et al., 1998). In the final stages of refinement, REFMAC5 (Murshudov et al., 1999) was used with a TLS description of B values, whereby the rigid groups were identified by automatic analysis of difference distance matrices (Schneider, 2002).

The structures were analyzed with Xfit, ESCET, and PROCHECK (Laskowski et al., 1993). Figures were made with PYMOL (http://pymol.sourceforge.net).

Supplemental Data

Supplemental Data include nine figures, three tables, and Supplemental Experimental Procedures and can be found with this article online at http://www.cell.com/cgi/content/full/124/6/1183/DC1/.

ACKNOWLEDGMENTS

We thank L. Hicke and S. Giordano for reagents; E. Cavallaro, V. Cecatiello, and M. Garre for technical assistance; A. Mattevi for providing X-ray facilities; C. Tarricone and R. Steiner for help in data collection; the staff of beamlines ID29 and BM14 at ESRF; and the Monoclonal Service at IFOM. This work was supported by grants from Associazione Italiana per la Ricerca sul Cancro (S.P., P.P.D.F., T.R.S., A.M.); Association for International Cancer Research (S.P.); European Community (VI Framework), Ministero della Salute, MIUR, Fondazione Monzino (P.P.D.F.).

Received: December 7, 2005
Revised: February 6, 2006
Accepted: February 14, 2006
Published online: February 16, 2006

REFERENCES

Alam, S.L., Sun, J., Payne, M., Welch, B.D., Blake, B.K., Davis, D.R., Meyer, H.H., Emr, S.D., and Sundquist, W.I. (2004). Ubiquitin interactions of NZF zinc fingers. EMBO J. *23*, 1411–1421.

Barbieri, M.A., Kong, C., Chen, P.I., Horazdovsky, B.F., and Stahl, P.D. (2003). The SRC homology 2 domain of Rin1 mediates its binding to the epidermal growth factor receptor and regulates receptor endocytosis. J. Biol. Chem. *278*, 32027–32036.

Bienko, M., Green, C.M., Crosetto, N., Rudolf, F., Zapart, G., Coull, B., Kannouche, P., Wider, G., Peter, M., Lehmann, A.R., et al. (2005). Ubiquitin-binding domains in Y-family polymerases regulate translesion synthesis. Science *310*, 1821–1824.

Brunger, A.T., Adams, P.D., Clore, G.M., DeLano, W.L., Gros, P., Grosse-Kunstleve, R.W., Jiang, J.S., Kuszewski, J., Nilges, M., Pannu, N.S., et al. (1998). Crystallography & NMR system: a new software suite for macromolecular structure determination. Acta Crystallogr. D Biol. Crystallogr. *54*, 905–921.

Chen, Z.J. (2005). Ubiquitin signalling in the NF-kappaB pathway. Nat. Cell Biol. *7*, 758–765.

Davies, B.A., Topp, J.D., Sfeir, A.J., Katzmann, D.J., Carney, D.S., Tall, G.G., Friedberg, A.S., Deng, L., Chen, Z., and Horazdovsky, B.F. (2003). Vps9p CUE domain ubiquitin binding is required for efficient endocytic protein traffic. J. Biol. Chem. *278*, 19826–19833.

Di Fiore, P.P., Polo, S., and Hofmann, K. (2003). When ubiquitin meets ubiquitin receptors: a signalling connection. Nat. Rev. Mol. Cell Biol. *4*, 491–497.

Donaldson, K.M., Yin, H., Gekakis, N., Supek, F., and Joazeiro, C.A. (2003). Ubiquitin signals protein trafficking via interaction with a novel ubiquitin binding domain in the membrane fusion regulator, Vps9p. Curr. Biol. *13*, 258–262.

Fazioli, F., Bottaro, D.P., Minichiello, L., Auricchio, A., Wong, W.T., Segatto, O., and Di Fiore, P.P. (1992). Identification and biochemical characterization of novel putative substrates for the epidermal growth factor receptor kinase. J. Biol. Chem. *267*, 5155–5161.

Fisher, R.D., Wang, B., Alam, S.L., Higginson, D.S., Robinson, H., Sundquist, W.I., and Hill, C.P. (2003). Structure and ubiquitin binding of the ubiquitin-interacting motif. J. Biol. Chem. *278*, 28976–28984.

Frank, D.J., Noguchi, T., and Miller, K.G. (2004). Myosin VI: a structural role in actin organization important for protein and organelle localization and trafficking. Curr. Opin. Cell Biol. *16*, 189–194.

Hama, H., Tall, G.G., and Horazdovsky, B.F. (1999). Vps9p is a guanine nucleotide exchange factor involved in vesicle-mediated vacuolar protein transport. J. Biol. Chem. *274*, 15284–15291.

Hicke, L., and Dunn, R. (2003). Regulation of membrane protein transport by ubiquitin and ubiquitin-binding proteins. Annu. Rev. Cell Dev. Biol. *19*, 141–172.

Hicke, L., Schubert, H.L., and Hill, C.P. (2005). Ubiquitin-binding domains. Nat. Rev. Mol. Cell Biol. *6*, 610–621.

Hofmann, K., and Falquet, L. (2001). A ubiquitin-interacting motif conserved in components of the proteasomal and lysosomal protein degradation systems. Trends Biochem. Sci. *26*, 347–350.

Horiuchi, H., Lippe, R., McBride, H.M., Rubino, M., Woodman, P., Stenmark, H., Rybin, V., Wilm, M., Ashman, K., Mann, M., and Zerial, M. (1997). A novel Rab5 GDP/GTP exchange factor complexed to Rabaptin-5 links nucleotide exchange to effector recruitment and function. Cell *90*, 1149–1159.

Kang, R.S., Daniels, C.M., Francis, S.A., Shih, S.C., Salerno, W.J., Hicke, L., and Radhakrishnan, I. (2003). Solution structure of a CUE-ubiquitin complex reveals a conserved mode of ubiquitin binding. Cell *113*, 621–630.

Karplus, K., Barrett, C., and Hughey, R. (1998). Hidden Markov models for detecting remote protein homologies. Bioinformatics *14*, 846–856.

Kawasaki, M., Shiba, T., Shiba, Y., Yamaguchi, Y., Matsugaki, N., Igarashi, N., Suzuki, M., Kato, R., Kato, K., Nakayama, K., and Wakatsuki, S. (2005). Molecular mechanism of ubiquitin recognition by GGA3 GAT domain. Genes Cells *10*, 639–654.

Krishna, S.S., Majumdar, I., and Grishin, N.V. (2003). Structural classification of zinc fingers: survey and summary. Nucleic Acids Res. *31*, 532–550.

Laskowski, R.A., MacArthur, M.W., Moss, D.S., and Thornton, J.M. (1993). PROCHECK: a program to check the stereochemical quality of protein structures. J. Appl. Crystallogr. *26*, 283–291.

Lee, S., Tsai, Y.C., Mattera, R., Smith, W.J., Kostelansky, M.S., Weissman, A.M., Bonifacino, J.S., and Hurley, J.H. (2006). Structural basis for ubiquitin recognition and autoubiquitination by Rabex-5. Nat. Struct. Mol. Biol., in press. Published online February 5, 2006. 10.1038/nsmb1064.

Mattera, R., Tsai, Y.C., Weissman, A.M., and Bonifacino, J.S. (2006). The Rab5 guanine nucleotide exchange factor Rabex-5 binds ubiquitin and functions as a ubiquitin ligase through an atypical UIM and a zinc finger domain. J. Biol. Chem., in press. Published online January 5, 2006. 10.1074/jbc.M509939200.

McRee, D.E. (1999). XtalView/Xfit—a versatile program for manipulating atomic coordinates and electron density. J. Struct. Biol. *125*, 156–165.

Miller, S.L., Malotky, E., and O'Bryan, J.P. (2004). Analysis of the role of ubiquitin-interacting motifs in ubiquitin binding and ubiquitylation. J. Biol. Chem. *279*, 33528–33537.

Morris, R.J., Perrakis, A., and Lamzin, V.S. (2002). ARP/wARP's model-building algorithms. I. The main chain. Acta Crystallogr. D Biol. Crystallogr. *D58*, 968–975.

Murshudov, G.N., Lebedev, A., Vagin, A.A., Wilson, K.S., and Dodson, E.J. (1999). Efficient anisotropic refinement of Macromolecular structures using FFT. Acta Crystallogr. D Biol. Crystallogr. *D55*, 247–255.

Ohno, A., Jee, J., Fujiwara, K., Tenno, T., Goda, N., Tochio, H., Kobayashi, H., Hiroaki, H., and Shirakawa, M. (2005). Structure of the UBA domain of Dsk2p in complex with ubiquitin molecular determinants for ubiquitin recognition. Structure (Camb.) *13*, 521–532.

Opipari, A.W., Jr., Boguski, M.S., and Dixit, V.M. (1990). The A20 cDNA induced by tumor necrosis factor alpha encodes a novel type of zinc finger protein. J. Biol. Chem. *265*, 14705–14708.

Otwinowski, Z., and Minor, W. (1997). Processing of X-ray diffraction data collected in oscillation mode. In Methods in Enzymology. Macromolecular Crystallography, Part A, C.W. Carter, Jr., and R.M. Sweet, eds. (San Diego, CA: Academic Press.), pp. 307–326.

Pickart, C.M. (2001). Ubiquitin enters the new millennium. Mol. Cell *8*, 499–504.

Polo, S., Confalonieri, S., Salcini, A.E., and Di Fiore, P.P. (2003). EH and UIM: endocytosis and more. Sci. STKE *2003*, re17.

Pornillos, O., Alam, S.L., Rich, R.L., Myszka, D.G., Davis, D.R., and Sundquist, W.I. (2002). Structure and functional interactions of the Tsg101 UEV domain. EMBO J. *21*, 2397–2406.

Prag, G., Misra, S., Jones, E.A., Ghirlando, R., Davies, B.A., Horazdovsky, B.F., and Hurley, J.H. (2003). Mechanism of ubiquitin recognition by the CUE domain of Vps9p. Cell *113*, 609–620.

Prag, G., Lee, S., Mattera, R., Arighi, C.N., Beach, B.M., Bonifacino, J.S., and Hurley, J.H. (2005). Structural mechanism for ubiquitinated-cargo recognition by the Golgi-localized, gamma-ear-containing, ADP-ribosylation-factor-binding proteins. Proc. Natl. Acad. Sci. USA *102*, 2334–2339.

Raasi, S., Orlov, I., Fleming, K.G., and Pickart, C.M. (2004). Binding of polyubiquitin chains to ubiquitin-associated (UBA) domains of HHR23A. J. Mol. Biol. *341*, 1367–1379.

Reverter, D., and Lima, C.D. (2005). Insights into E3 ligase activity revealed by a SUMO-RanGAP1-Ubc9-Nup358 complex. Nature *435*, 687–692.

Schneider, T.R. (2002). A genetic algorithm for the identification of conformationally invariant regions in protein molecules. Acta Crystallogr. D Biol. Crystallogr. *D58*, 195–208.

Sessa, F., Mapelli, M., Ciferri, C., Tarricone, C., Areces, L.B., Schneider, T.R., Stukenberg, P.T., and Musacchio, A. (2005). Mechanism of Aurora B activation by INCENP and inhibition by hesperadin. Mol. Cell *18*, 379–391.

Sheldrick, G.M. (2002). Macromolecular phasing with SHELXE. Z. Kristallogr. *217*, 644–650.

Shih, S.C., Katzmann, D.J., Schnell, J.D., Sutanto, M., Emr, S.D., and Hicke, L. (2002). Epsins and Vps27p/Hrs contain ubiquitin-binding domains that function in receptor endocytosis. Nat. Cell Biol. *4*, 389–393.

Shih, S.C., Prag, G., Francis, S.A., Sutanto, M.A., Hurley, J.H., and Hicke, L. (2003). A ubiquitin-binding motif required for intramolecular monoubiquitylation, the CUE domain. EMBO J. *22*, 1273–1281.

Sigismund, S., Woelk, T., Puri, C., Maspero, E., Tacchetti, C., Transidico, P., Di Fiore, P.P., and Polo, S. (2005). Clathrin-independent endocytosis of ubiquitinated cargos. Proc. Natl. Acad. Sci. USA *102*, 2760–2765.

Song, J., Zhang, Z., Hu, W., and Chen, Y. (2005). Small ubiquitin-like modifier (SUMO) recognition of a SUMO binding motif: a reversal of the bound orientation. J. Biol. Chem. *280*, 40122–40129.

Sun, L., and Chen, Z.J. (2004). The novel functions of ubiquitination in signaling. Curr. Opin. Cell Biol. *16*, 119–126.

Sundquist, W.I., Schubert, H.L., Kelly, B.N., Hill, G.C., Holton, J.M., and Hill, C.P. (2004). Ubiquitin recognition by the human TSG101 protein. Mol. Cell *13*, 783–789.

Swanson, K.A., Kang, R.S., Stamenova, S.D., Hicke, L., and Radhakrishnan, I. (2003). Solution structure of Vps27 UIM-ubiquitin complex important for endosomal sorting and receptor downregulation. EMBO J. *22*, 4597–4606.

Tall, G.G., Barbieri, M.A., Stahl, P.D., and Horazdovsky, B.F. (2001). Ras-activated endocytosis is mediated by the Rab5 guanine nucleotide exchange activity of RIN1. Dev. Cell *1*, 73–82.

Varadan, R., Assfalg, M., Haririnia, A., Raasi, S., Pickart, C., and Fushman, D. (2004). Solution conformation of Lys63-linked di-ubiquitin chain provides clues to functional diversity of polyubiquitin signaling. J. Biol. Chem. *279*, 7055–7063.

Wang, B., Alam, S.L., Meyer, H.H., Payne, M., Stemmler, T.L., Davis, D.R., and Sundquist, W.I. (2003). Structure and ubiquitin interactions of the conserved zinc finger domain of Npl4. J. Biol. Chem. *278*, 20225–20234.

Wertz, I.E., O'Rourke, K.M., Zhou, H., Eby, M., Aravind, L., Seshagiri, S., Wu, P., Wiesmann, C., Baker, R., Boone, D.L., et al. (2004). De-ubiquitination and ubiquitin ligase domains of A20 downregulate NF-kappaB signalling. Nature *430*, 694–699.

Yokouchi, M., Kondo, T., Houghton, A., Bartkiewicz, M., Horne, W.C., Zhang, H., Yoshimura, A., and Baron, R. (1999). Ligand-induced ubiquitination of the epidermal growth factor receptor involves the interaction of the c-Cbl RING finger and UbcH7. J. Biol. Chem. *274*, 31707–31712.

Accession Numbers

The coordinates and structure factors have been deposited in the Protein Data Bank (accession codes 2C7M and 2C7N).